



Towards explaining the Nd paradox using reversible scavenging in an ocean general circulation model

Mark Siddall^{a,*}, Samar Khatiwala^a, Tina van de Flierdt^{a,b,1}, Kevin Jones^{a,b}, Steven L. Goldstein^{a,b}, Sidney Hemming^{a,b}, Robert F. Anderson^{a,b}

^a Lamont-Doherty Earth Observatory of Columbia University, 61 Route 9W, Palisades, NY 10964, USA

^b Department of Earth and Environmental Sciences, Columbia University, New York, NY 10027, USA

ARTICLE INFO

Article history:

Received 18 April 2008

Received in revised form 25 July 2008

Accepted 29 July 2008

Available online 7 September 2008

Editor: M.L. Delaney

Keywords:

neodymium

REE

MOC

reversible scavenging

ABSTRACT

The isotopic composition of the rare earth element neodymium (Nd) has the potential to serve as water-mass tracer, because it is naturally tagged by continental sources with distinct ages and lithologies. However, in order to understand the limitations of this approach we need to know more about the physical and biogeochemical processes controlling the distribution of Nd in the modern ocean. For example, Nd isotope ratios behave quasi-conservatively, while concentrations in the water column generally increase with depth, showing a broadly nutrient-like behaviour. We define this decoupling of Nd concentrations and isotopic compositions as the “Nd paradox”. For the first time we model Nd concentrations and isotopic compositions simultaneously and address the hypothesis that the Nd paradox can be explained by a combination of lateral advection and reversible scavenging. We impose a reversible-scavenging model of Nd removal from the ocean on the ocean circulation fields from the MIT general circulation model using the transport matrix method. We conclude that reversible scavenging is an active and important component in the cycling of Nd in the ocean. In the absence of an adequate alternative explanation, reversible scavenging should be considered a necessary component in explaining the Nd paradox.

© 2008 Elsevier B.V. All rights reserved.

1. Introduction

1.1. The neodymium isotopic composition as a tracer for water-mass mixing

Different water masses in the ocean are characterised by distinct Nd isotopic compositions, the values of which are ultimately derived from the continents and delivered to the ocean through weathering, erosion, and particle–seawater interaction (Piepgras et al., 1979; Goldstein and O’Nions, 1981; Frank, 2002; Tachikawa et al., 2003; Goldstein and Hemming, 2003; Lacan and Jeandel, 2005). ^{143}Nd is produced by radioactive decay of ^{147}Sm , and $^{143}\text{Nd}/^{144}\text{Nd}$ in seawater is primarily a function of the age and lithology of the continental sources. Because this ratio only varies in the third or fourth digit, it is usually expressed as ϵ_{Nd} , the parts per 10,000 deviation of a measured $^{143}\text{Nd}/^{144}\text{Nd}$ ratio from the “bulk Earth” value of 0.512638 (Jacobsen and Wasserburg, 1980).

In the global oceans two principal end members for dissolved Nd isotopic compositions are recognized. North Atlantic Deep Water (NADW) ($\epsilon_{\text{Nd}} = -13.5 \pm 0.5$; Piepgras and Wasserburg, 1987) has low

values reflecting the old continental crust surrounding the North Atlantic. Deep water in the North Pacific has higher values ($\epsilon_{\text{Nd}} = -2$ to -4 ; for recent summaries see van de Flierdt et al., 2004 and Goldstein and Hemming, 2003) reflecting contributions from young volcanic arcs. Intermediate Nd isotopic compositions are found in Circum-Antarctic and Indian Ocean deep waters (Piepgras and Wasserburg, 1980, 1982; Bertram and Elderfield, 1993). Because Nd has an ocean residence time of ~ 200 – 2000 yr (Goldstein and O’Nions, 1981; Piepgras and Wasserburg 1983; Jeandel, 1993; Tachikawa et al., 1999; Tachikawa et al., 2003), long enough to be transported within the global thermohaline circulation system and short enough to avoid complete homogenisation, Nd isotope ratios in seawater have been used to trace water masses in the present and past ocean.

The potential use of Nd isotopes as a water-mass tracer is supported by a compilation of Nd isotope seawater measurements from the Atlantic Ocean, which appear to trace the distribution of water masses in the basin (i.e. NADW; Antarctic Intermediate Water, AAIW, and; Antarctic Bottom Water, AABW) (von Blanckenburg, 1999). The co-variation of Nd isotopes with water-mass tracers such as salinity is corroborated on a global scale (Goldstein and Hemming, 2003). These findings serve as the basis for the view that Nd isotopes can serve as a “quasi-conservative water-mass tracer” (see recent summaries in Frank, 2002; Goldstein and Hemming, 2003).

Recently, Piotrowski et al. (2005) reconstructed the first high-resolution record of Nd isotopes in the authigenic fraction of marine

* Corresponding author. Now at the Department of Earth Sciences, University of Bristol, Wills Memorial Building, Queen’s Road, Bristol, BS8 1RJ, United Kingdom.

E-mail address: siddall@ideo.columbia.edu (M. Siddall).

¹ Now at the Department of Earth Science and Engineering, Imperial College London, South Kensington Campus, London SW7 2AZ, United Kingdom.

sediments from the Cape Basin (SE Atlantic) for the last glacial cycle, with the goal to reconstruct the strength of the Atlantic meridional overturning circulation over this interval. The record was produced by the preferential dispersal of Nd from the ferro-manganese oxide fraction of bulk sediments by sequential leaching of discrete samples from cores RC11-83 and TN057-21. The authors suggest that the variations in the record correlate with Greenland paleo-temperature, indicating that the fraction of NADW-derived Nd reaching the Southern Ocean increased during warm northern hemisphere interglacial and interstadial intervals and was reduced during glacial and stadial intervals (Rutberg et al., 2000; Piotrowski et al., 2004, 2005). Arsouze et al. (2008) suggested that these variations could be explained by changes to the ϵ_{Nd} value of NADW instead of changes to NADW intensity but this seems incompatible with the results of van de Flierdt et al. (2006) who found that the ϵ_{Nd} value of NADW was stable over the last glacial period.

There is obvious potential of Nd isotopes as a tool for understanding past changes in ocean circulation. However, any application of Nd isotopes as a circulation tracer, whether in the present or the past ocean, suffers from considerable gaps in existing knowledge about sources, sinks and internal cycling of Nd in seawater. Here we aim to address some of these issues by testing the importance of reversible scavenging for the marine Nd cycle in an ocean general circulation model for the first time.

1.2. Sources of neodymium to the ocean and the “neodymium paradox”

Although it is established that the continents are the major source of Nd to the ocean, the transport pathways of neodymium and how water masses acquire their neodymium isotopic composition are still unresolved (e.g., Frank, 2002; Goldstein and Hemming, 2003; van de Flierdt et al., 2004; Lacan and Jeandel, 2005). It has been shown that hydrothermal sources do not contribute to the dissolved seawater Nd budget in any significant way due to immediate removal of hydrothermal Nd at the vent site (e.g., Goldstein and O’Nions, 1981; Piepgras and Wasserburg, 1985; German et al., 1990; Halliday et al., 1992) but there is an ongoing debate on the relative importance of riverine versus aeolian sources of Nd to the ocean. The magnitudes of both fluxes are associated with considerable uncertainties due to removal (and remobilization) of Nd in estuaries on the one hand, and unknown dissolution rates of Nd from dust on the other hand (see Frank, 2002; van de Flierdt et al., 2004 for recent summaries). Applying literature estimates of global riverine and atmospheric fluxes from the 1990s, however, leads to a calculated residence time of Nd in the ocean on the order of 5000 yr (Bertram and Elderfield, 1993). This is not considered realistic because pronounced Nd isotopic differences are observed between water masses and large inter-basin gradients exist (e.g., Piepgras et al., 1979; Goldstein and O’Nions, 1981). These inter-basin gradients provide strong evidence for a residence time for Nd on the order of, or shorter than, the global turnover time of the ocean (1000 to 1500 yr; Broecker and Peng, 1982). These calculations indicate a missing source of Nd to the ocean, leading some authors to term this mass balance problem the “Nd paradox” (e.g., Bertram and Elderfield, 1993; Jeandel et al., 1995; see also van de Flierdt et al., 2004). Here we address, instead, the alternative definition of Goldstein and Hemming (2003), who state it as “the decoupling of Nd concentrations and isotopic compositions in the ocean”. Concentrations of Nd and other Rare Earth Elements in all the major ocean basins are relatively depleted in surface waters and enriched in deep waters, and there is an overall increase in concentrations from the North Atlantic to the North Pacific. With respect to these characteristics the concentrations of REEs follow a broadly similar distribution to silicate or phosphate in the ocean (e.g., Elderfield, 1988), and clearly are not conservative by the classical chemical oceanography definition. Neodymium isotopic compositions on the other hand are very distinct between the different ocean basins,

and they show a pronounced structure in the water column which closely follows the distribution of deep-ocean water masses, giving Nd isotopes a ‘quasi-conservative’ character. For the purpose of this work, we will refer to the Nd paradox as the general mismatch between Nd isotopes, which tag water masses, and Nd concentrations, which reflect the internal cycling of Nd in the ocean.

No matter how we define the Nd paradox, whether in terms of mass balance, or in terms of a decoupling of concentrations and isotopes, the observational data clearly point to additional sources, sinks, and/or processes that play an important role in the oceanic Nd cycle. The observed distribution of Nd isotopes in seawater from the North Pacific is an interesting case in point. The high Nd isotope ratios found in this part of the ocean ($\epsilon_{\text{Nd}} = -2$ to -6 ; Piepgras and Wasserburg, 1980; Piepgras and Jacobsen, 1988; Shimizu et al., 1994; Amakawa et al., 2000, 2004; Vance et al., 2004) can be explained neither by input from large rivers nor from dust, as both of these sources exhibit more negative ϵ_{Nd} values than those associated with dissolved Nd in the North Pacific (see van de Flierdt et al., 2004 for a detailed discussion). To achieve an isotopic mass balance, local volcanic arcs must be a major source of Nd in the North Pacific, although, the mechanisms by which the Nd is added to the ocean remains unclear. For example, the input may involve interaction of river particulates with seawater, input of volcanic ash, and near bottom dissolution of deposited or resuspended sediments at the continent/ocean interface (e.g., Albarède and Goldstein, 1992; Elderfield and Sholkovitz, 1987; Spivack and Wasserburg, 1988; Bertram and Elderfield, 1993; Jeandel et al., 1995, 1998; Sholkovitz et al., 1999; Amakawa et al., 2000, 2004; Sholkovitz and Szymczak, 2000; Lacan and Jeandel, 2001, 2005). The importance of direct input via the flux of volcanic ash into the ocean may be amplified by the fact that volcanic ash is much more readily dissolved than continental material (e.g., Taylor and McLennan, 1985). Recently it has been suggested that submarine groundwater discharge may be a mechanism for introducing arc-like Nd to the ocean (Johannesson and Burdige, 2007).

Taking supply of Nd from the boundaries into account, Tachikawa et al. (2003) could calculate a residence time of 500 yr for Nd from box-model simulations of Nd concentrations in the global ocean. However, it has also been noted that water masses may interact with ocean margins to change their ϵ_{Nd} signature without additional input of Nd from the margin (Lacan and Jeandel, 2005). Lacan and Jeandel (2005) suggested the term “boundary exchange” to explain the alteration of isotope ratios at the ocean margins that cannot be accounted for by additional Nd input while acknowledging that the direct mechanism of this exchange reaction is not yet understood.

Here we will not address the detailed issues of Nd input to the ocean. Instead we focus on the internal cycling of Nd in the ocean. Our working hypothesis is that the quasi-conservative behaviour of Nd isotopes in deep waters along with increasing neodymium concentrations as water ages may be explained by a combination of lateral advection and vertical cycling via reversible scavenging. Here we will test this hypothesis for the first time.

2. Method

2.1. Reversible scavenging

In an attempt to resolve the Nd paradox, we have applied the reversible-scavenging model of Bacon and Anderson (1982) to Nd isotope concentrations. Reversible scavenging is the process of isotope adsorption onto particles with subsequent desorption due to the release of the isotope during dissolution, particle aggregation/disaggregation, or variation in the dissolved isotope concentration. Note that the process of reversible scavenging relies on the physical process of particle adsorption/desorption onto particles and should not be confused with biological incorporation of REE. The use of a reversible-scavenging model for investigating the internal cycling of

Table 1
List of variables and units

<i>Variables relating to Nd</i>		
[Nd]	pmol kg ⁻¹	Nd concentration
ε _{Nd}	–	Nd isotope ratio normalised to standard
<i>Variables relating to reversible scavenging</i>		
C	pmol kg ⁻¹	Total tracer concentration
C _p	pmol kg ⁻¹	Particle-associated concentration
C _d	pmol kg ⁻¹	Dissolved tracer concentrations
w _s	m yr ⁻¹	Particle settling velocity
K	–	Scavenging coefficient
R	–	Particulate concentration
S	–	The product of K and R
z	m	Depth
<i>Variables relating to the TMM (see Khatiwala, 2007 for details)</i>		
L	–	Physical transport (advection, convection, diffusion)
q	–	Representation of reversible scavenging
t	s	Time
A _e	–	The TM for the explicit-in-time component of advection–diffusion
A _i	–	The matrix for implicit transport
Q	–	Sparse matrix representation of reversible scavenging

Nd in the ocean is justified by the observation that Nd concentrations generally increase with depth (e.g. de Baar et al., 1985), a common characteristic of isotopes that are reversibly scavenged. In the case of Nd, concentrations increase down the water column primarily because of the dissolution of particles with depth (see Section 2.2).

Reversible scavenging in the model can be described as follows. At a give time step, the total Nd concentration is first transported via the ocean model, which includes advective, convective and diffusive transport. The total Nd concentration is then divided into particle-associated and dissolved constituents. This separation into particle-associated and dissolved Nd depends on the particle concentration and type, as detailed below. The particle-associated Nd sinks at a given rate, along with the particle it is associated with while the dissolved Nd remains at the same depth level.

The inclusion of reversible scavenging into an ocean model (see Section 2.4) is accomplished as follows: if we write the conservation equation for a tracer with total concentration C as:

$$\frac{\partial C}{\partial t} = L(C) + q(C), \quad (1)$$

where L represents the physical circulation, then the objective is to represent (parameterize) q in terms of the simulated tracer concentration. $q(C)$ represents internal (vertical) cycling in the water column. All variables listed in this paper are summarised in Table 1. Following from Henderson et al. (1999), Marchal et al. (2000) and Siddall et al. (2005, 2007) this formulation only considers particle concentrations it does not take into account particle size distributions.

To simulate reversible scavenging we use an equilibrium-scavenging coefficient to describe the relationship between adsorbed and desorbed isotopes. That is, each isotope is assumed to be in equilibrium with falling particles. Such equilibrium-scavenging coefficients have often been used to describe the relationship between adsorbed and desorbed ²³¹Pa and ²³⁰Th (Henderson et al., 1999; Chase et al., 2002; Siddall et al., 2005, 2007, 2008). The dimensionless equilibrium-scavenging coefficient, K , is defined as the ratio between dissolved, C_d , and particle-associated, C_p , concentrations of a given isotope:

$$K = \frac{C_p}{C_d R}, \quad (2)$$

where R is the dimensionless ratio of the particle mass per cubic meter to the density of the fluid. For the purpose of this study we will denote Nd concentrations as [Nd] in units of pmol kg⁻¹. We will assume that no isotopic fractionation occurs during adsorption/desorption, i.e., K values are the same for ¹⁴³Nd and ¹⁴⁴Nd. This is

justified in this case because ¹⁴³Nd and ¹⁴⁴Nd are isotopes of a similar, heavy mass and, most importantly, are isotopes of the same element (unlike ²³¹Pa and ²³⁰Th). For scavenging by falling particles, we can write the source term as:

$$q(C) = -\frac{\partial(w_s C_p)}{\partial z}, \quad C = [S/(S+1)]C, \quad (3)$$

where, w_s is the particle settling velocity and S is the product of K and R (i.e. KR).

Different particle types are known to have different K values for ²³¹Pa and ²³⁰Th (see for example Chase et al., 2002). K values are likely to be specific to different particle types for other elements, such as Nd. This effect is included in Eq. (3) by substituting S to allow for differences in particle type. S is defined as:

$$S = K_{\text{POC}}R_{\text{POC}} + K_{\text{CaCO}_3}R_{\text{CaCO}_3} + K_{\text{dust}}R_{\text{dust}} + K_{\text{Opal}}R_{\text{Opal}}, \quad (4)$$

after Siddall et al. (2005).

2.2. A note on reversible scavenging of Nd with emphasis on the effect of particle dissolution

Reversible scavenging has been invoked to model the behaviour of ²³¹Pa and ²³⁰Th in the ocean. However, these isotopes have a fundamentally different input mechanism compared to ¹⁴³Nd and ¹⁴⁴Nd. ²³¹Pa and ²³⁰Th are input to the ocean via decay from a homogeneously distributed parent isotope. This means that the input of ²³¹Pa and ²³⁰Th in the ocean are evenly distributed at all points in the ocean and this input must be balanced by removal to satisfy conservation. Removing ²³¹Pa and ²³⁰Th from the ocean therefore requires that the isotopes which are input at all points in the ocean are integrated with respect to depth via the process of reversible scavenging. In contrast, the input of Nd isotopes to seawater is predominantly of continental origin and occurs largely at the surface of the ocean. Away from continental sources (including dust input to the surface ocean) there are no additional sources of Nd besides lateral and vertical transport (unlike ²³¹Pa and ²³⁰Th). Because Nd input to the ocean occurs largely at the surface, conservation requires that the removal of Nd in the ocean (i.e. the downward flux of Nd via reversible scavenging) is equal to the flux of Nd into the surface. Unlike the case of ²³¹Pa and ²³⁰Th, the vertical integration of Nd sources at depth is not required because such sources do not exist. Because the vertical Nd flux due to reversible scavenging depends on the particle-associated [Nd] (C_p), the implication is that C_p must be uniform with respect to depth. Note that this outcome assumes that the settling velocity is uniform with respect to depth. This is an assumption of our model but is not necessarily the case in the ocean itself.

Given this implication, we briefly investigate the effect of reversible scavenging on Nd distributions in the ocean. Rearranging Eq. (2) gives us:

$$C_d = \frac{C_p}{S} = \frac{C_p}{KR}. \quad (5)$$

Because the particle concentration, R , reduces with depth and K and C_p remain constant C_d must increase with depth. This implies that [Nd] in the water column is sensitive to the specific nature of particle dissolution profiles in different regions of the ocean. The dissolution profiles imposed here are derived from independent studies of marine and surface sediment dissolution (see e.g. Henderson et al., 1999) and so we keep them fixed. We vary the scavenging coefficients (K values in Eqs. (4) and (5)) for different particle types. In regions where dissolution is more significant there will be a greater increase in C_d with respect to depth. In regions where dissolution is less significant C_d will tend to be more uniform with respect to depth (e.g. in the deep Pacific, below the Gobi dust plume because dust is not highly soluble).

If scavenging was not reversible, i.e. if dissolution did not release Nd adsorbed onto particles into the water column, then the profiles of [Nd] in

the ocean would not increase with depth and [Nd] would tend to be uniform with respect to depth. This condition would be required to conserve Nd in the ocean as non-reversible scavenging transported Nd down the water column. In areas of more vigorous horizontal transport (i.e. in the Atlantic), transport of Nd within water-mass trajectories would mean that [Nd] would track water masses. This is indeed the case in the model simulations we have carried out. These simulations are not shown in the paper because there is little gained from showing results with no variation in the vertical axis besides the overprint of transport along water-mass trajectories in the North Atlantic. In the case of ϵ_{Nd} such simulations are effectively the same as those described by Jones et al. (2008).

2.3. Particle fields

Following Siddall et al. (2005, 2007, 2008), biogenic particle fields are prescribed using satellite-derived export productivity fields and appropriate dissolution profiles for three particle types: biogenic opal; $CaCO_3$ and; particulate organic carbon (POC) (Behrenfeld and Falkowski, 1997; Laws et al., 2000; Maier-Reimer, 1993). The surface dust input field is taken from the Global Ozone Chemistry Aerosol Radiation and Transport (GOCART) model simulations (Ginoux et al., 2001). Each particle type dissolves differentially with respect to depth and temperature and so each is discussed separately. Fig. 1A–D shows

the particle fluxes from the surface used in the model simulations as well as the fluxes at 2000 m depth.

Particle dissolution in the model is similar to that discussed in detail by Henderson et al. (1999), Marchal et al. (2000) and Siddall et al. (2005). As discussed by Henderson et al. (1999), these dissolution profiles were derived by comparison to existing sediment trap data for particle concentrations and have been tested in many ocean models. We briefly summarise these below: dissolution of $CaCO_3$ and opal with respect to depth are described by an exponential penetration profile (after Henderson et al., 1999) and dissolution of POC with respect to depth is described by a power law. Dust is assumed to not dissolve significantly with respect to depth. We assume that the dissolution of trace metals associated with surface dust input does not significantly affect the total dust concentration. Similar to previous work (Henderson et al., 1999; Marchal et al., 2000; Siddall et al., 2005, 2007), particles are subject to a uniform settling rate of 1000 m yr^{-1} across all particle types – no distinction in settling rate is made for particles of different size classes. Given that the residence time of Nd in the ocean is hundreds of years we apply an annual mean settling rate, which does not allow for rapid ‘marine snow’ events but captures the mean particle flux to the sediment. Distributions of scavenged trace elements in the equilibrium-scavenging model have no sensitivity to changes in settling rate because of the nature of the formulation of this model (see Siddall et al., 2005; 2008).

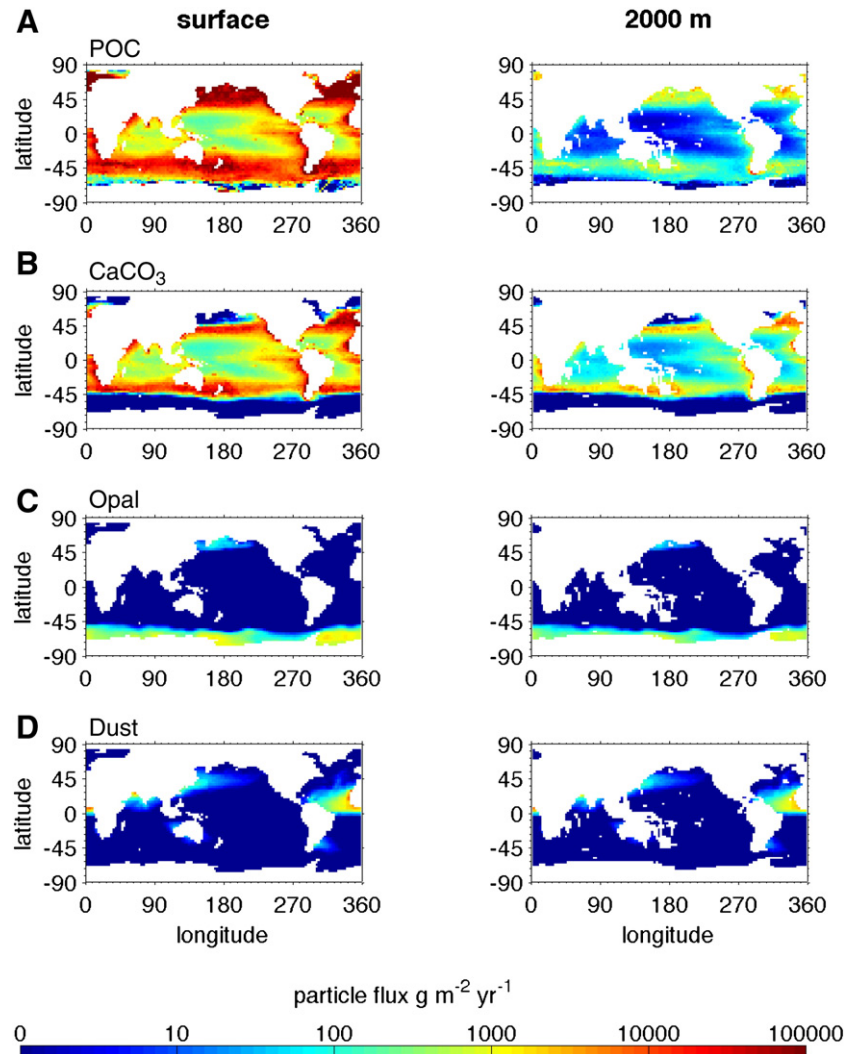


Fig. 1. The total flux of particles from the ocean surface and at 2000 m depth imposed on the model in $\text{g m}^{-2} \text{ yr}^{-1}$ for each of the four particle types. Following Siddall et al. (2005), biogenic particle fields are prescribed using satellite-derived export productivity fields for three particle types: biogenic opal; $CaCO_3$ and; particulate organic carbon (POC) (Behrenfeld and Falkowski, 1997; Laws et al., 2000; Maier-Reimer, 1993). The surface dust input field is taken from the Global Ozone Chemistry Aerosol Radiation and Transport (GOCART) model simulations (Ginoux et al., 2001).

Opal dissolution in surface sediment provides 79–94% of the silicic acid input to the ocean (Treguer et al., 1995; Ridgwell et al., 2002). The global mean dissolution rate of CaCO_3 in surface sediment is of the order of 70–80% (Archer 1996; Ridgwell and Hargreaves, 2007). In order to capture these effects in our model we follow the dissolution profiles described in the paragraph above but then impose a dissolution of 85% for opal, 75% for CaCO_3 and 95% for POC in the model boxes which juxtapose the sea floor. The effect of allowing sea-floor dissolution on the model results will be explored in Section 3.4.2.

2.4. Transport matrix model

To compute steady state solutions of the tracer equation (Eq. (1)) with a prescribed surface boundary condition, we use an “offline” ocean circulation model based on the “transport matrix method” (TMM) of Khatiwala et al., 2005 (see also Khatiwala, 2007). The TMM is a computational framework for efficiently simulating passive tracers in the ocean. The essential idea is that the discrete tracer transport operator of an ocean general circulation model (GCM) can be written as a sparse matrix, which may be efficiently constructed by “probing” the GCM with idealized basis functions. In essence this approach generates a high-resolution, dynamically consistent box model of tracer transport in the ocean. This empirical approach ensures that the circulation embedded in the transport matrix (TM) accurately represents the complex 3-dimensional advective–diffusive transport (including all sub-grid scale parameterizations) of the underlying GCM. Once the matrix has been derived, the GCM can be dispensed with and simulating a tracer is reduced to a sequence of simple matrix–vector products. Specifically, in the TM formulation, the discrete version of Eq. (1) becomes:

$$c^{n+1} = A_i[A_e c + q(c)]. \quad (6)$$

Here, c is a vector of tracer concentrations at the grid points of the underlying GCM, i.e., a vector representation of a discretized 3-dimensional tracer field; n is the time step index; A_e the TM for the explicit-in-time component of advection–diffusion; and A_i the matrix for implicit transport (see Khatiwala, 2007 for details).

One of the key advantages of using the TMM is that it allows us to directly compute steady state solutions of the tracer equations without the need for lengthy transient integrations, as would be required with a GCM or a conventional offline tracer model. Specifically, given surface boundary conditions and (optionally) interior source/sink terms, the steady state tracer distribution satisfies a linear system of equations that can be readily solved using software such as MATLAB. To apply the TMM to the present problem, we note that the reversible-scavenging term $q(C)$ (Eq. (3)) is linear in C , and can (in discrete form) be written as Q_c , where Q is a sparse matrix. The steady state solution to Eq. (5) with a prescribed surface boundary condition (see Section 2.5) can then be obtained by splitting A_e , A_i , and Q into “interior” and “boundary” matrices, by extracting the rows and columns corresponding to interior and boundary points, respectively:

$$c^I = [A_i^I(A_e^I + Q^I) - I]^{-1} [A_i^B(B_e + Q^B) + B_i] c^B. \quad (7)$$

The superscripts I and B refers to “interior” and “boundary”, respectively. Thus, c^I is the desired vector of interior tracer concentrations in steady state, and c^B the vector of prescribed surface boundary values. Using Eq. (7), we can rapidly compute the equilibrium distribution of Nd isotopes for different boundary conditions and scavenging coefficients (embedded in Q).

The TM used in this study was derived from a seasonally forced, global configuration of the MIT ocean model, a state-of-the-art primitive equation model (Marshall et al., 1997). The MIT GCM features a variety of parameterizations to represent unresolved processes, including isopycnal thickness diffusion (Gent and McWilliams, 1990) to represent the effect of mesoscale eddies. The configuration used here has a horizontal resolution of 2.8° and 15 vertical levels, and is forced with monthly mean

climatological fluxes of momentum (Trenberth et al., 1989) and heat (Jiang et al., 1999). In addition, surface temperature and salinity are weakly restored to the Levitus climatology (Levitus, 1998). To compute steady state solutions of the tracer equations with the TMM, the GCM was first integrated for 5000 yr to equilibrium, following which an annual mean transport matrix was derived.

This version of the model has previously been used as MIT’s contribution to the Ocean Carbon Model Inter-comparison Project Phase 2 (OCMIP-2), and further details, including an extensive discussion of its ability to reproduce observed CFC and radiocarbon distributions, can be found in Dutay et al. (2002) and Matsumoto et al. (2004). Briefly, the model tends to be more rapidly ventilated in both the North Pacific and subpolar North Atlantic, compared with observations, while it has relatively weak bottom water ventilation around Antarctica. These deficiencies in the model circulation are a common problem for coarse resolution GCMs.

2.5. The Nd surface boundary condition

The issue of Nd input to the ocean has been discussed extensively in the literature (see Section 1). In terms of modelling several approaches have been used — explicit sources estimated from observational studies have been used in box models for both $[\text{Nd}]$ and ε_{Nd} (Tachikawa et al., 2003; Lacan and Jeandel 2005; Arsouze et al., 2007). In addition Lacan and Jeandel (2005) and Arsouze et al. (2007) prescribed ε_{Nd} terms at the ocean margins to which they applied a ‘boundary exchange’ model, which may be compared to a restoring condition on oceanic ε_{Nd} values imposed at the ocean margin with a certain restoring time scale. We focus on internal cycling of Nd in the open ocean, rather than on the sources of Nd at the ocean margins or the exchange of ^{143}Nd and ^{144}Nd with the boundaries. Therefore, we choose to impose fixed surface boundary conditions on Nd isotope concentrations in our ocean model (c^B in Eq. (7)). It should be noted that our prescribed surface boundary condition is consistent with the available data and therefore represents to some extent all the complex and still unresolved processes that input Nd to the ocean without dealing with them explicitly.

Recently Jones et al. (in press) used an interpolation of observed surface ε_{Nd} values in order to generate a fixed surface boundary condition for use in their model. They use the relatively scarce surface ε_{Nd} data in the surface model layer in conjunction with interpolation schemes in an attempt to account for all the isotope variation in the surface ocean. We also prescribe a fixed surface boundary condition but in addition to ε_{Nd} data we also need observations of Nd concentration ($[\text{Nd}]$). Observations used throughout this paper are of dissolved $[\text{Nd}]$. Ideally for this study observations of dissolved $[\text{Nd}]$ would be at the same sites as ε_{Nd} observations but unfortunately this is seldom the case and sites where both ε_{Nd} and dissolved $[\text{Nd}]$ observations are both present are rare in the upper 200 m of the water column. To circumvent this problem, we define surface boxes and take mean ε_{Nd} and dissolved $[\text{Nd}]$ observations from within them. We then use these mean values to calculate ^{143}Nd and ^{144}Nd surface concentrations in the boxes.

The sparse data for surface dissolved $[\text{Nd}]$ combined with uncertainty concerning the input of Nd to the ocean leads to a large number of possible variations in the way we define the surface boxes. We have chosen to use a small number of boxes, each with a large number of observations to constrain the $[\text{Nd}]$ and ε_{Nd} that are then used in the resulting surface boundary condition for each box (Fig. 2A,B). Although we have adopted this approach to maximise the number of surface observations in each box there are several large regions with poor data coverage where only a small number of observations in the upper 200 m of the water column constrain the surface values. This is an issue that can only be addressed by additional observational work in the future. We should note that our approach differs from that of Jones et al. (in press), who also apply the TMM to model Nd isotopes in the ocean. Similar to Arsouze et al. (2007), they treat ε_{Nd} as a conservative tracer with a prescribed surface distribution. In contrast, we separately model the individual isotope concentrations.

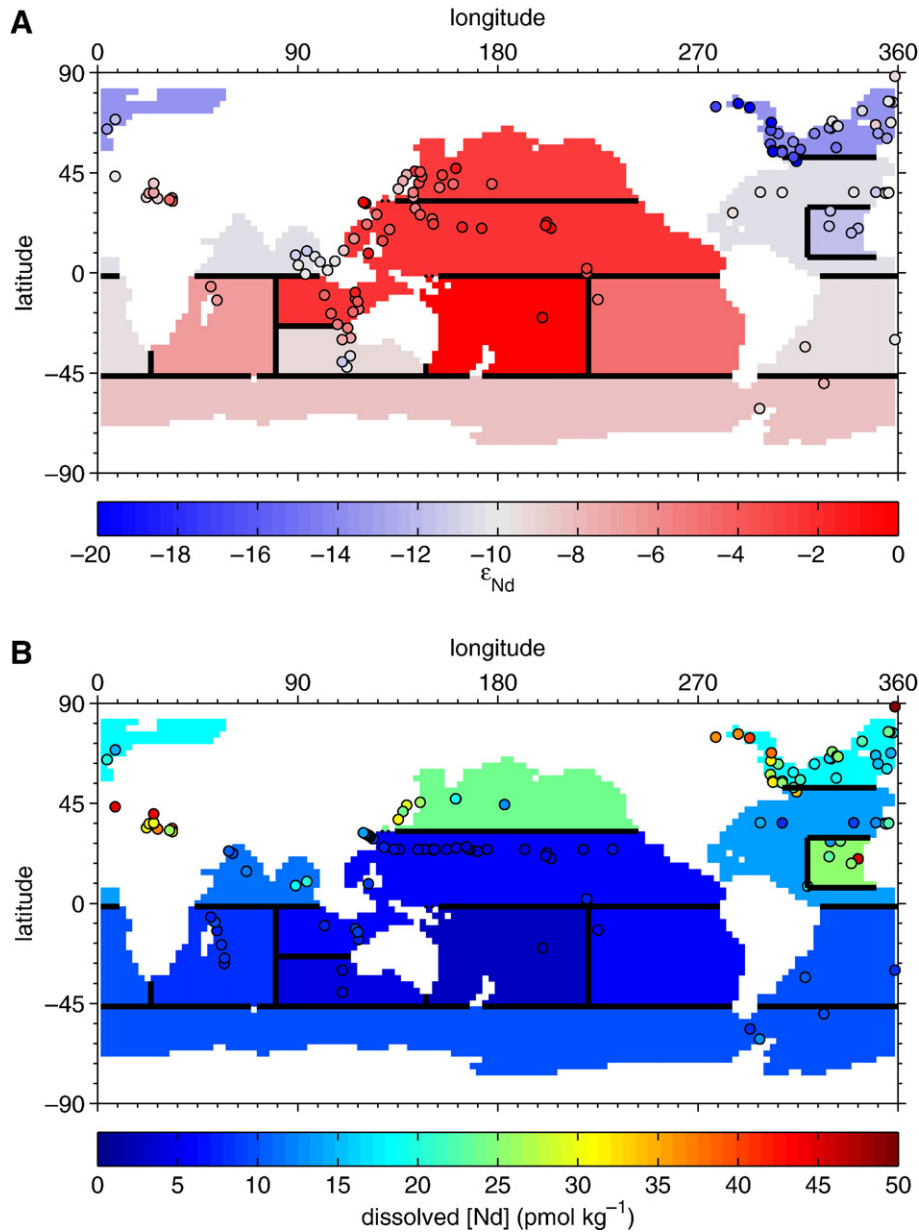


Fig. 2. The surface boundary condition for ϵ_{Nd} (A) and the dissolved Nd concentration [Nd] (B) used for the simulations shown in this paper. The data, shown as colored circles, are mean values of profiles for the upper 200 m from the compilation by F. Lacan and T. van de Fliedert; http://www.legos.obs-mip.fr/fr/equipes/geomar/results/database_may06.xls; see also Jones et al. (in press) for references. Additional [Nd] observations are from Greaves et al. (1999), Elderfield and Greaves (1982), Piepgras and Jacobsen (1992), Bertram and Elderfield (1993), Shimizu et al. (1994) and German et al. (1995). The values used in each box are the based on the means of all data from the upper 200 m of the water column. Observations with concentrations greater than 25 pmol kg^{-1} in the high-latitude North Atlantic (above 50°N) are considered to result from being very close to the source and not representative of open-ocean values. Therefore these values are ignored. Similarly high [Nd] values in the North-west Pacific are ignored. Values that appear to occur over land are from marginal seas and are not used to derive the surface boundary condition but are simply included here for completeness. (For interpretation of the references to color in this figure legend, the reader is referred to the web version of this article.)

Because of the relatively long residence time of Nd in the ocean compared to the mixing time of ocean gyres, the supply of Nd which is imposed at the surface becomes well mixed across ocean gyres below the top hundred meters in most of the ocean. This apparent mixing in the upper water column means that taking the average values from the surface in each of the ocean gyres gives an adequate representation of Nd transfer from the upper to the deep ocean for the purpose of this study. For much of the ocean there is little sensitivity to exactly what we prescribe at the surface except on spatial scales on the order of, or larger than, ocean gyres. One exception to this statement is the prescribed boundary condition in the high-latitude North Atlantic in the regions of NADW formation and this is discussed below.

Several authors have noted the sensitivity of the global Nd distribution to input in the N. Atlantic (Frank, 2002; Tachikawa et al., 2003; Lacan and Jeandel, 2005; Arsouze et al., 2007) and the mixing processes between end members from the Norwegian Sea and Labrador Sea. Mixing of Labrador Sea and Norwegian Sea water masses and the precise location of high-latitude convection are poorly understood in general and poorly represented in coarse resolution GCMs. This general limitation of many contemporary ocean models should be kept in mind when interpreting the results presented here. This issue is confounded by the effects of boundary exchange, which are not explicitly considered in our model, but are believed to affect the ϵ_{Nd} in the high-latitude North Atlantic (Lacan and Jeandel, 2005;

Arsouze et al., 2007). In order to avoid this problem we ignore observations close to boundaries in this region (i.e. within several hundred kilometers from the coast) and instead focus only on observations away from the margins. The mean of these values yields $[\text{Nd}]$ and ε_{Nd} values that are representative of those of NADW. Using this data filter the ε_{Nd} and $[\text{Nd}]$ values in NADW are successfully simulated which lend support to this approach.

The goal of this study is to investigate the extent to which reversible scavenging can explain the Nd paradox, rather than to explain all of the unknowns regarding the sources of Nd to the ocean. Therefore, although the surface boundary condition might not be strictly correct, we consider this simplification adequate for this application.

2.6. Model tuning and sensitivity

2.6.1. Tuning the model scavenging parameters

To tune the model for the effects of reversible scavenging on the Nd system, we consider the effect of varying the equilibrium-scavenging coefficients, K values, on the distribution of $[\text{Nd}]$ and ε_{Nd} in the ocean, the residence time of Nd in the ocean and on a simple cost function (σ)

which defines the root-mean squared deviation of the data from the model (TMMRS):

$$\sigma_i = \sqrt{\sum (data_i - TMMRS)^2} \quad (8)$$

data represents the dataset of dissolved $[\text{Nd}]$ or ε_{Nd} , as denoted by the subscript i . Because reversible scavenging operates primarily on $[\text{Nd}]$ and generates ε_{Nd} as a bi-product, we focus on $\sigma_{[\text{Nd}]}$ and use any comparison with ε_{Nd} as an independent validation of the method. The dataset used throughout this paper is from seawater analyses of Nd isotopes based on Lacan and Jeandel (2005), with additional compilation by Francois Lacan, and Tina van de Fliert: http://www.legos.obs-mip.fr/fr/equipes/geomar/results/database_may06.xls; see also Jones et al. (in press) for references. Additional dissolved $[\text{Nd}]$ observations are from Greaves et al. (1999), Elderfield and Greaves (1982), Piepgras and Jacobsen (1992), Bertram and Elderfield (1993), Shimizu et al. (1994) and German et al. (1995).

In order to estimate K_{POC} , K_{CaCO_3} , K_{dust} and K_{Opal} , we use the function 'lsqcurvefit' in the MATLAB optimisation toolbox. This function uses a least-squares approach to minimise $\sigma_{[\text{Nd}]}$ in Eq. (8)

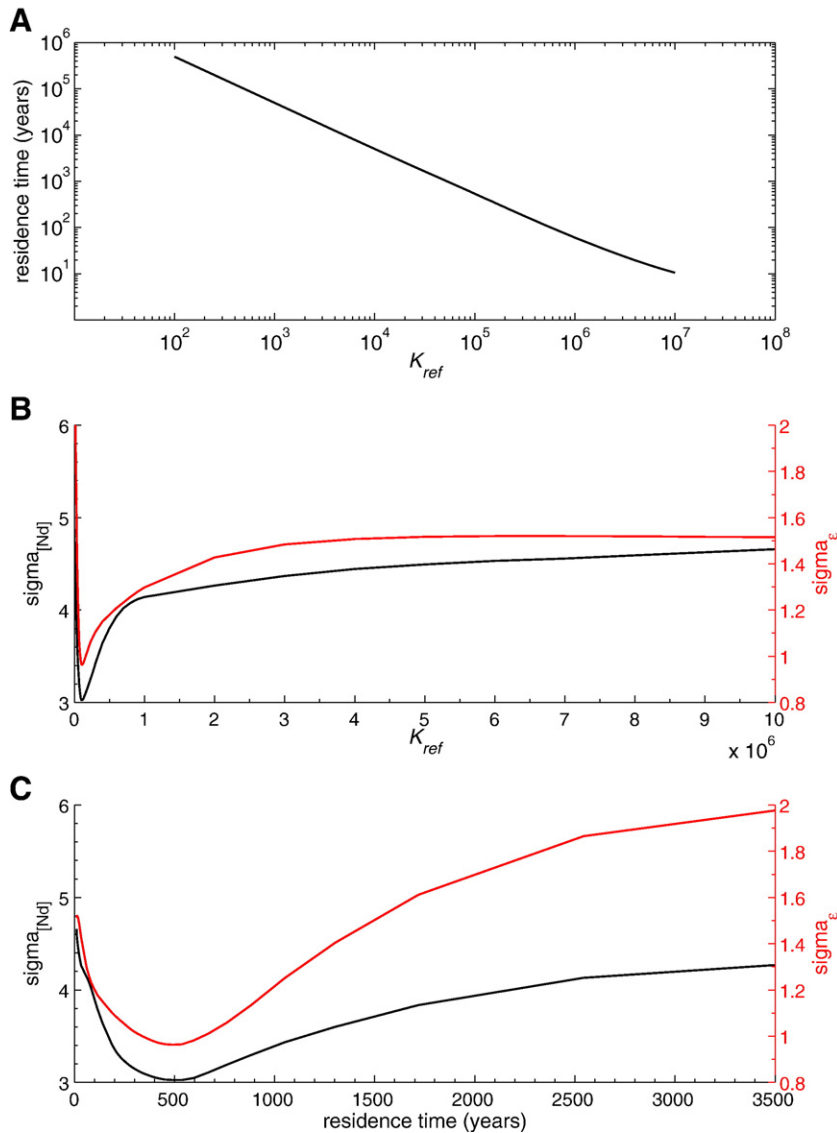


Fig. 3. Sensitivity of the model to varying K_{ref} for the control simulation, where scavenging coefficients were optimised for each particle type to fit the dissolved $[\text{Nd}]$ (i.e. minimising $\sigma_{[\text{Nd}]}$). The panels display the sensitivity of residence time to K_{ref} (panel A), the sensitivity of the cost functions to varying K_{ref} (panel B), and the sensitivity of the cost functions to the corresponding residence time. Panels A and B have dual y-axes with display σ_{ε} and $\sigma_{[\text{Nd}]}$, as indicated on axis labels. It is significant that σ_{ε} and $\sigma_{[\text{Nd}]}$ are both optimised for the same K_{ref} value and residence time.

by selecting optimal values for K_{POC} , K_{CaCO_3} , K_{dust} and K_{Opal} . Optimum values are found for: $K_{\text{POC}}=0.0 \times 10^5$; $K_{\text{CaCO}_3}=2.1 \times 10^5$; $K_{\text{dust}}=28.9 \times 10^5$ and; $K_{\text{Opal}}=6.0 \times 10^5$. We define the simulation using these values as the control. The variation of K of one order of magnitude for different particle types is similar to the variation of K values for ^{231}Pa and ^{230}Th (Chase et al., 2002). The optimum solution implies that there is effectively no scavenging of Nd by POC. This result can only be considered tentative in this exploratory study because the dissolution profiles of CaCO_3 and POC are relatively similar (i.e. compared to the dissolution profiles of opal and dust) and it is quite possible that the model optimum fit is biased towards attributing scavenging to CaCO_3 , which is more correctly attributable to POC. Furthermore the precise quantification of the scavenging coefficients presented here is dependent on the surface boundary condition and dissolution profiles imposed on the model. The optimal solution indicates that K_{dust} is an order of magnitude greater than the other K values. This contrasts with the scavenging of ^{231}Pa and ^{230}Th by dust, which is much lower than scavenging by other particle types (Siddall et al., 2005). Therefore the finding that K_{dust} for Nd is relatively high is somewhat surprising. Scavenging coefficients vary greatly between different elements and this may explain why the optimal K_{dust} for Nd is relatively high. Alternatively the explanation could be due to uncertainties in the dust fluxes imposed on the model, which can be large (Ginoux et al., 2001). It should be kept in mind that the goal of this paper is an exploratory study into the impact of reversible scavenging on the Nd cycle in the ocean, rather than a fully quantitative study.

The results in the paragraph above suggest that there is a strong dependence of particle type on the scavenging of Nd in the ocean. We are not aware of independent, observational constraints on the scavenging coefficients of different particle types but emphasise that such constraints are greatly needed. In the absence of better constraints on surface dissolved [Nd] the scavenging coefficients presented in this paper can only be regarded as tentative.

2.6.2. Sensitivity of ocean residence time to K

In order to consider the sensitivity of the residence time of Nd in the model to variations scavenging intensity we define a reference K value, $K_{\text{ref}}=1 \times 10^5$, so that $K_{\text{POC}}=0 \times K_{\text{ref}}$, $K_{\text{CaCO}_3}=2.1 \times K_{\text{ref}}$, $K_{\text{dust}}=28.9 \times K_{\text{ref}}$ and $K_{\text{Opal}}=6.0 \times K_{\text{ref}}$ for the control simulation. Fig. 3A shows the effect on the ocean residence time of varying K_{ref} .

Reducing K_{ref} reduces the rate at which Nd is removed to the ocean sediments and increases the ocean residence time, which in turn enhances the effects of horizontal transport via ocean transport processes. Increasing K_{ref} has the opposite effect. Increasing K_{ref} increases the rate at which Nd is transported down the water column. This reduces the effects of lateral transport and vertical transport via reversible scavenging dominates.

We define the residence time as the time taken to totally remove Nd from the ocean, so that Nd release during opal dissolution from the sea floor is accounted for. Very similar optimum K_{ref} and residence times are found for both $\sigma_{[\text{Nd}]}$ and σ_ε of ~ 500 yr (Fig. 3B,C). Because both $\sigma_{[\text{Nd}]}$ and σ_ε are minimised for this same residence time we are confident that this value is reasonable. Note that Tachikawa et al. (2003) also estimated a residence time of 500 yr for Nd in the ocean.

The K_{ref} used here is 1×10^5 , in comparison K value of approximately 1×10^7 (estimated for ^{230}Th) leads to a residence time of 10–30 yr, and a K value of approximately 1×10^6 (estimated for ^{231}Pa) leads to a residence time of 100 yr (see e.g. Marchal et al., 2000).

3. Results

3.1. Comparison of model results with the global dataset

In order to compare our model results with observations we plot our model results for both dissolved [Nd] and ε_{Nd} against observations for the case where scavenging coefficients were optimised for each

particle type (tuned to minimise σ_{Nd} , Fig. 4A,B). The data from different ocean basins are represented by different colors and symbols.

It is clear that the model captures the broad-scale (inter-basin, inter-gyre) variability in the global ocean. This is the case for both dissolved [Nd] and ε_{Nd} . The fit between model and observations is reasonable (i.e. most of the data falls within $1 \varepsilon_{\text{Nd}}$ unit) throughout the ocean for dissolved [Nd] but the Atlantic comparisons are better than the Pacific for ε_{Nd} . The offsets between model and observations for ε_{Nd} in the Pacific are due to the simplified surface boundary condition used in the model, which does not represent specific features such as the very positive ε_{Nd} values observed in the proximity of Hawaii and other highly radiogenic sources of Nd (see Jones et al., in press for further discussion). Nevertheless, 72% of the Pacific and 90% of the Atlantic model-data comparisons fall within $1 \varepsilon_{\text{Nd}}$ of the observed values.

We emphasise that the model is tuned to optimise the fit to dissolved [Nd] (i.e. by minimising $\sigma_{[\text{Nd}]}$). The fact that the model represents ε_{Nd} reasonably well is an independent check on our approach. This should be borne in mind as one considers the detailed comparisons of model simulation and observations below.

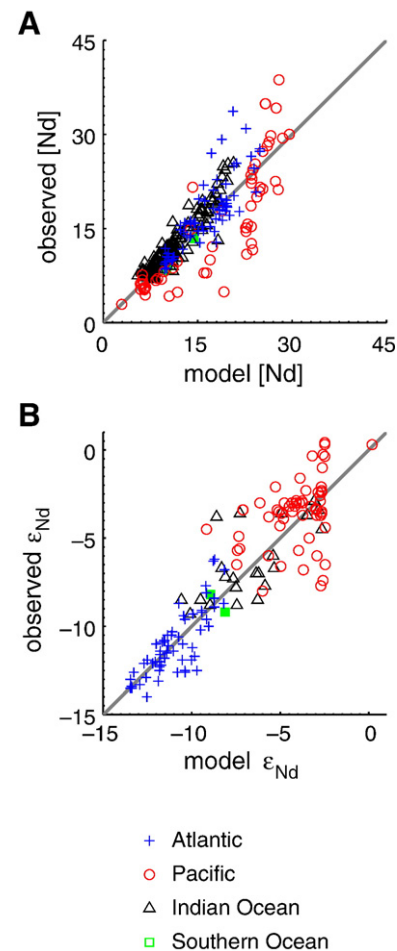


Fig. 4. Direct comparison of model and data for ε_{Nd} (A) and dissolved [Nd] (B) in different ocean basins (see key on plot) at all depth levels for the case where scavenging coefficients were optimised for each particle type. Data shown are published seawater analyses of Nd isotopes based on Lacan and Jeandel (2005), with additional compilation by Francois Lacan, and Tina van de Fliedert: http://www.legos.obs-mip.fr/fr/equipes/geomar/results/database_may06.xls; see also Jones et al. (in press) for references. Additional [Nd] observations are from Greaves et al. (1999), Elderfield and Greaves (1982), Piepgras and Jacobsen (1992), Bertram and Elderfield (1993), Shimizu et al. (1994) and German et al. (1995). Atlantic data do not include observations from the high-latitude North Atlantic ($>50^\circ\text{N}$), where boundary scavenging may play a dominant role. The offset in the Pacific in ε_{Nd} is due to the simplified surface boundary condition used in the model, which does not capture specific features such as the very positive ε_{Nd} values observed in the proximity of Hawaii and other highly radiogenic sources of Nd.

3.2. [Nd] and ϵ_{Nd} at the sea floor

We now consider [Nd] and ϵ_{Nd} at the sea floor (i.e. the deepest model box for each horizontal grid square, Fig. 5A,B). In agreement with observations, more positive ϵ_{Nd} values dominate the deep Pacific and more negative values dominate the deep Atlantic (Fig. 5A). The Indian and Southern Oceans display intermediate values. Note that ϵ_{Nd} values from manganese crusts are included to help characterise the large-scale, inter-basin differences in a qualitative sense. Values for ϵ_{Nd} from manganese crusts are not reliable in an absolute sense

because manganese crusts accumulate very slowly so that their ϵ_{Nd} values integrate long term, glacial to interglacial variability.

Nd tends to accumulate in the deep, North Pacific, as can be observed by the high dissolved [Nd] there. Dissolved [Nd] is lowest in the Atlantic while the Indian and Southern Ocean have intermediate dissolved [Nd]. The accumulation of Nd in the deep Pacific is in agreement with the observation that dissolved [Nd] co-varies with dissolved nutrient concentrations (see, for example, Goldstein and Hemming, 2003).

The inter-basin patterns in both ϵ_{Nd} values and dissolved [Nd] are in good agreement with observations.

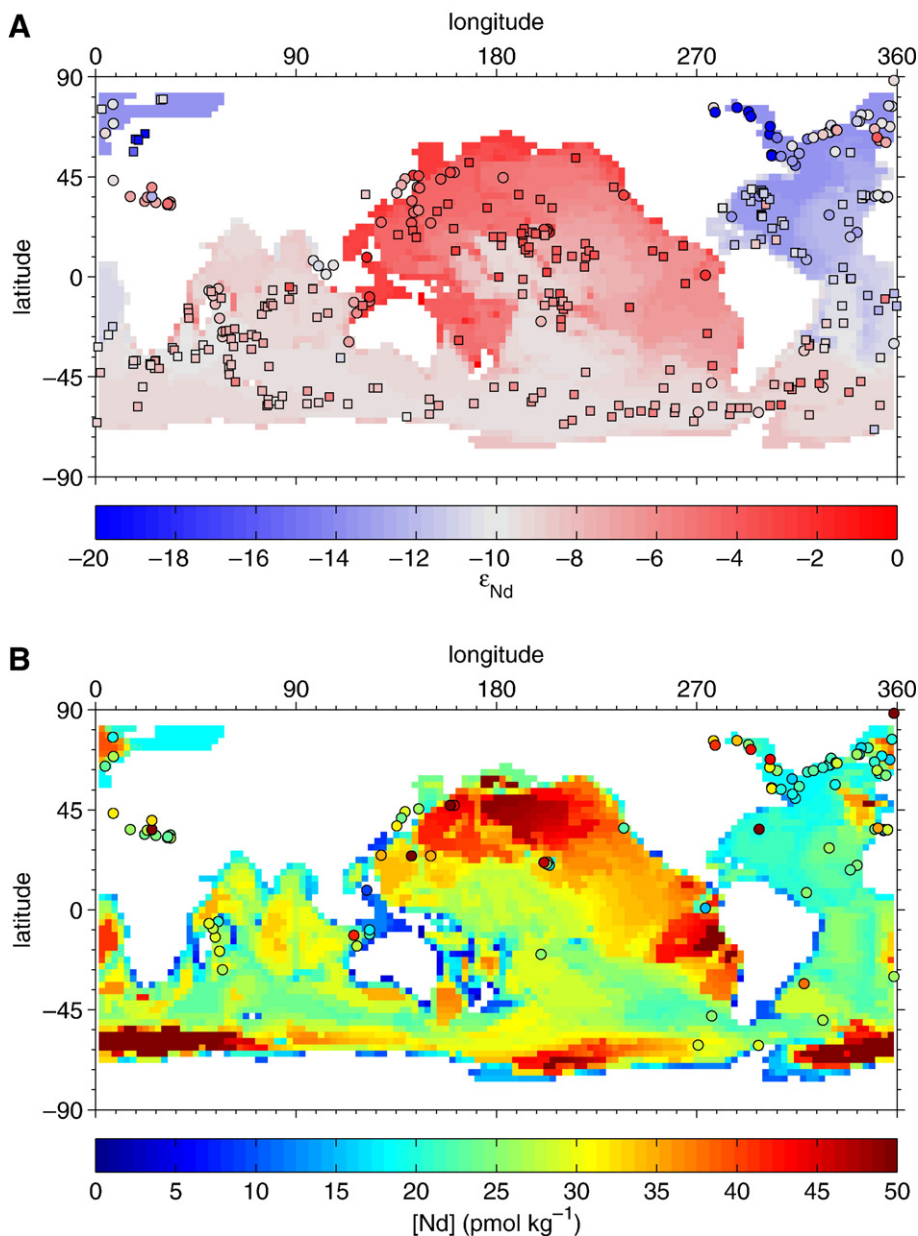


Fig. 5. ϵ_{Nd} (A) and the dissolved [Nd] (B) in the deepest box of the model at each grid point for the control simulation, where scavenging coefficients were optimised for each particle type. The thickness of the model grid increases from 50 m at the surface to 690 m at the deepest box. Observations for the deepest 1000 m of the water column are shown as colored circles (water-column data are published seawater analyses of Nd isotopes based on Lacan and Jeandel, 2005, with additional compilation by Francois Lacan, and Tina van de Fliert: http://www.legos.obs-mip.fr/fr/equipements/geomar/results/database_may06.xls; see also Jones et al., in press for references. Additional [Nd] observations are from Greaves et al., 1999, Elderfield and Greaves, 1982, Piepgras and Jacobsen, 1992, Bertram and Elderfield, 1993, Shimizu et al., 1994 and German et al., 1995). Observations of ϵ_{Nd} on manganese crusts are shown as colored squares in A and are from the database of Frank (2002). The manganese nodule data represent the integration of long periods of time (potentially several glacial cycles) and are included only as an indication of the large-scale, inter-basin variability. Observations that appear to occur over land are from marginal seas and are not in this work. They are simply included here for completeness. (For interpretation of the references to color in this figure legend, the reader is referred to the web version of this article.)

3.3. [Nd] and ϵ_{Nd} along basin transects

We now compare an Atlantic transect along 336°E and a Western Pacific transect along 184°E as well as profiles of dissolved [Nd] and ϵ_{Nd} in comparison with observational data (Figs. 6A–D and 7A–D). The red lines in each of the depth profiles mark the model output for the control simulation introduced in Section 2.6.1 and are compared with observed water-column profiles in the following subsections.

3.3.1. The Atlantic

First we compare ϵ_{Nd} for the optimised simulation in the Atlantic Ocean with observational data from the same ocean basin (Fig. 6A). The general comparison is good – modelled ϵ_{Nd} trace water masses, in agreement with observations. The consideration of specific water-column profiles of ϵ_{Nd} allows a more detailed comparison of model and data (Fig. 6B). The model simulates the observed variability in each water-column profile well – the observed variation along each profile is simulated by the model and the simulation is typically within 1 ϵ_{Nd} unit of the observations.

We now compare dissolved [Nd] for the optimised simulation in the Atlantic Ocean with observational data (Fig. 6C). Again, the general

comparison is good – modelled dissolved [Nd] increases with depth, in agreement with observations. Specific water-column profiles of dissolved [Nd] are shown in Fig. 6D. The model simulates the observed variability in each water-column profile well, particularly in the South Atlantic, where dissolved [Nd] increases steadily with depth (in quantitative agreement with observed values) but ϵ_{Nd} shows the details of local water-mass distributions.

In the North Atlantic, the model output represents the interaction of multiple processes: reversible scavenging; input of Nd from the Saharan dust plume at around 5 to 25°N (Tachikawa et al., 1999; Bayon et al., 2004); vigorous water-mass transport; and scavenging by Saharan dust. Moving from top to bottom of the [Nd] water-column profiles in the North Atlantic below the Saharan dust plume (second and third profiles from the right in Fig. 6D), one can identify several key features:

1. The Nd input from the Saharan dust plume is quickly released to the dissolved phase in the upper water column (Tachikawa et al., 1999; Bayon et al., 2004) so that dissolved [Nd] peaks at the surface.
2. This Nd is mixed laterally across the North Atlantic gyre. Below the surface, dissolved [Nd] reduces towards values that represent [Nd] within subsurface water masses.

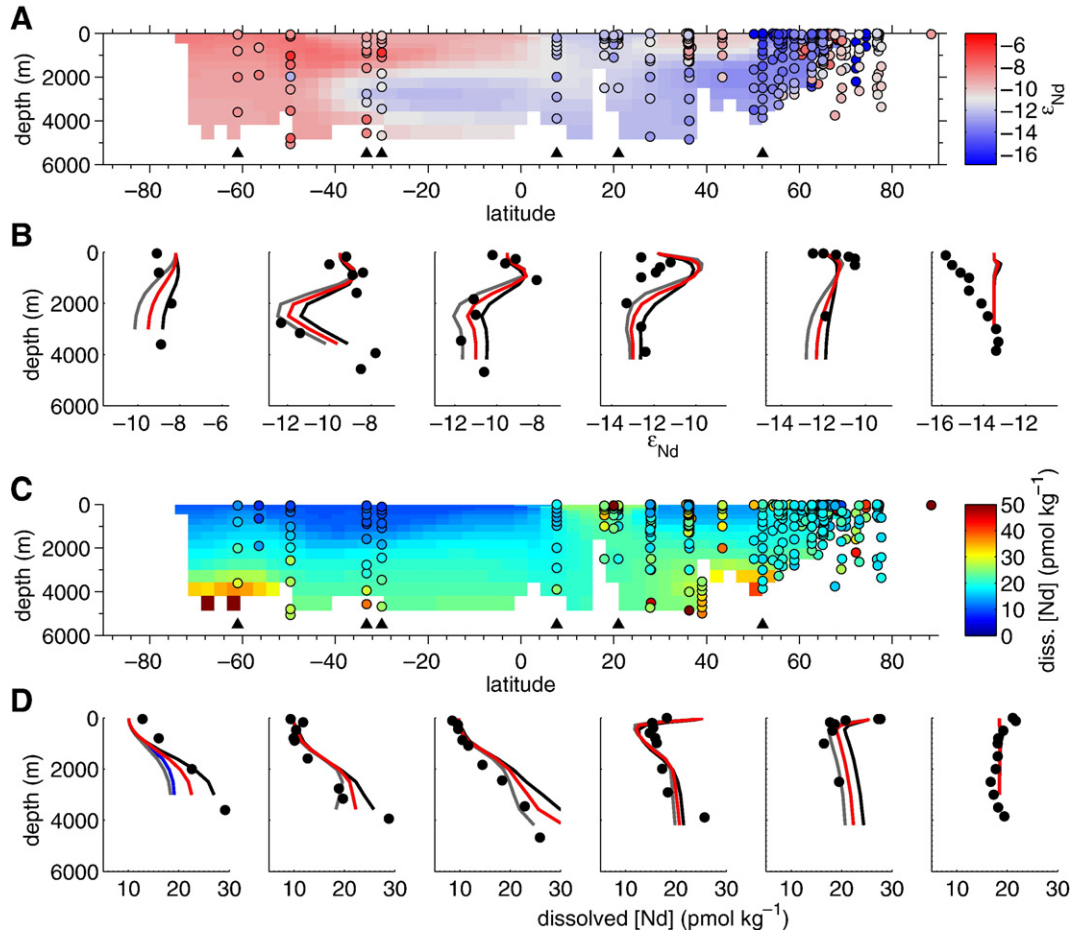


Fig. 6. Atlantic transects for the control simulation along 336°E and Atlantic profiles. A and B show ϵ_{Nd} . C and D show dissolved [Nd]. Water-column data are shown as colored circles on transects (A and C) and as black dots on the vertical profiles (C and D). Water-column data are published seawater analyses of Nd isotopes based on Lacan and Jeandel (2005), with additional compilation by Francois Lacan, and Tina van de Flierdt: http://www.legos.obs-mip.fr/fr/equipages/geomar/results/database_may06.xls; see also Jones et al. (in press) for references. Additional [Nd] observations are from Elderfield and Greaves (1982); and; German et al. (1995). The latitude of each of the profiles (C and D) is shown by the black triangles at 5500 m on the transects (A and C) in left to right order. Again in left to right order the references for each of the profiles is: Piepgras and Wasserburg (1982, 1987) (1st, 5th and 6th); Jeandel (1993) (2nd, 3rd and 4th). The lines on the profiles (C and D) are as follows: red lines represent the best fit run ($K_{ref} = 1 \times 10^5$); grey lines represent $K_{ref} = 0.5 \times 10^5$ and black lines represent $K_{ref} = 1.5 \times 10^5$. Little difference is observed in the profiles of ϵ_{Nd} for different values of K_{ref} . Black lines in C and D have larger deep dissolved [Nd] values for increased K_{ref} (i.e. $K_{ref} = 1.5 \times 10^5$) and grey lines have reduced deep dissolved [Nd] for decreased K_{ref} (i.e. $K_{ref} = 0.5 \times 10^5$). The blue line in the leftmost profile of D represents the simulation where no sea-floor dissolution was permitted. (For interpretation of the references to color in this figure legend, the reader is referred to the web version of this article.)

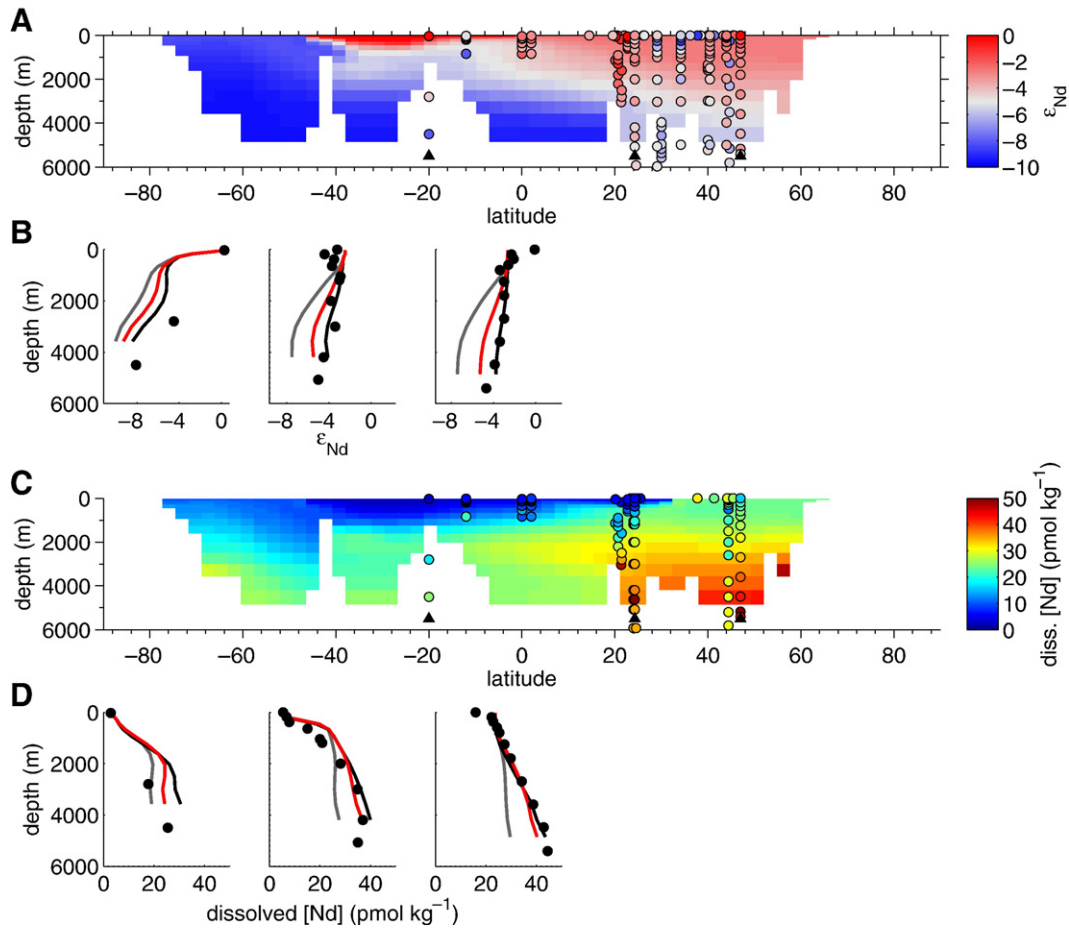


Fig. 7. Pacific transects along 184°E and Pacific profiles for the control simulation. A and B show ϵ_{Nd} . C and D show dissolved [Nd]. Water-column data are shown as colored circles on transects (A and C) and as black dots on the vertical profiles (C and D). Water-column data are published seawater analyses of Nd isotopes based on Lacan and Jeandel (2005), with additional compilation by Francois Lacan, and Tina van de Fliedert: http://www.legos.obs-mip.fr/fr/equipes/geomar/results/database_may06.xls; see also Jones et al. (in press) for references. Additional [Nd] observations are from Greaves et al. (1999) and Shimizu et al. (1994). The latitude of each of the profiles (C and D) is shown by the black triangles at 5500 m on the transects (A and C) in left to right order. The data for each of the profiles is from Piegras and Jacobsen (1992). The lines on the profiles (C and D) are as follows: red lines represent the best fit run ($K_{\text{ref}}=1 \times 10^5$); grey lines represent $K_{\text{ref}}=0.5 \times 10^5$ and black lines represent $K_{\text{ref}}=1.5 \times 10^5$. Little difference is observed in the profiles of ϵ_{Nd} for different values of K_{ref} . Black lines in C and D have larger deep dissolved [Nd] values for increased K_{ref} (i.e. $K_{\text{ref}}=1.5 \times 10^5$) and grey lines have reduced deep dissolved [Nd] for decreased K_{ref} (i.e. $K_{\text{ref}}=0.5 \times 10^5$). (For interpretation of the references to color in this figure legend, the reader is referred to the web version of this article.)

3. Scavenging by dust works to homogenise the dissolved [Nd] profiles beneath the Saharan dust plume (i.e. reduce the increase in dissolved [Nd] with depth). This is because dust does not significantly dissolve with respect to depth and therefore does not release Nd at depth (see Section 2.2 for a discussion of this effect).

These processes are each captured by the model and explain the observed patterns in dissolved [Nd] in the North Atlantic.

Below the dust plume, modelled ϵ_{Nd} shows a generally good comparison with data (second and third profiles from the right in Fig. 6B). However, at 10°N, between 500 and 1000 m water depths (third profile from the right in Fig. 6B) the model gives higher ϵ_{Nd} values than observed. This implies that Nd transport via NADW in the model may be weaker than reality.

In the northernmost profile shown in Fig. 6 (Fig. 6B and D, rightmost profile) ϵ_{Nd} observations show reduced values at the surface, which increase with depth. Observed dissolved [Nd] is lowest in the middle of the water column and peaks close to the sea floor and at the surface. We attribute this complicated pattern to the detailed nature of deep-water formation and boundary exchange/input in this region (Lacan and Jeandel, 2005; Arsouze et al., 2007). Our model is not configured to capture this complexity and so the model output shows the impact of vigorous vertical convection on both ϵ_{Nd} and dissolved [Nd] – both are close to uniform in the vertical axis in the control simulation.

3.3.2. The Pacific

If we compare ϵ_{Nd} for the control simulation in the Pacific Ocean with data (Fig. 7A), the general comparison of model data and observational data is good. At depth, modelled ϵ_{Nd} is lower in the South Pacific compared to the north, in agreement with observations. Specific water-column profiles of ϵ_{Nd} are shown in Fig. 7B, allowing a more detailed comparison of model and data. The model simulates the observed variability in each water-column profile well – the observed variation along each profile is simulated by the model and the simulation is typically within 1 ϵ_{Nd} unit of the observations.

Next we compare dissolved [Nd] for the optimised simulation in the Atlantic with data (Fig. 7C). The general comparison is good – modelled dissolved [Nd] generally increases with depth, in agreement with observations. Specific water-column profiles of dissolved [Nd] are shown in Fig. 7D. The model simulates the observed variability in each water-column profile well – the simulated increase in dissolved [Nd] with depth agrees quantitatively with observed values.

The middle profile of the three dissolved [Nd] profiles in the Pacific in Fig. 7D does not show an increase with depth in a simple, linear fashion like the profiles of dissolved [Nd] in the South Pacific or South Atlantic (Fig. 6D). Instead both model and observation profiles show large increases in [Nd] in the upper several thousand meters of the water column. Because this pattern is similar for both the model and

the observations, the model may give some insight into why this might be the case. The model suggests that this is because particulate CaCO_3 concentrations are relatively high at the surface but low at depth, where dust concentrations are relatively high. This means that CaCO_3 dominates reversible scavenging in the upper several thousand meters and dissolved [Nd] increases with depth due to the dissolution of CaCO_3 . Below the upper several thousand meters most of the CaCO_3 has been dissolved and scavenging by dust from the Gobi dust plume dominates. Because dust does not substantially dissolve with respect to depth the increase of dissolved [Nd] with depth is reduced in the lower water column in the proximity of the Gobi dust plume in the Pacific (see Section 2.2 for a discussion of this effect).

In both the Atlantic and the Pacific, the profiles of dissolved [Nd] closely follow the form predicted by the release of adsorbed Nd at depth due to reversible scavenging (Figs. 6D and 7D). We note that the downward transport of ϵ_{Nd} signatures is more important in the Pacific, where lateral transport via water masses is reduced, compared to the Atlantic. Jones et al. (in press) found that an additional source of Nd with high ϵ_{Nd} in the deep Pacific is required to explain the observed distribution of ϵ_{Nd} . We tentatively suggest that high ϵ_{Nd} in the deep North Pacific could be partly explained by a high ϵ_{Nd} input at the surface (e.g. at the volcanic arcs), which is scavenged to the sea floor by either the high dust and/or the high opal flux in the region. This concept is further supported by the relatively high scavenging coefficients found for dust and opal. This suggestion is tentative because we are cautious not to over interpret results that may be model dependent, in particular with respect to the simplified surface boundary condition we apply.

In Fig. 6B the southernmost of the three profiles for ϵ_{Nd} (Fig. 6B leftmost profile) shows lower values at depth than at the surface but the detail of the comparison is relatively poor and the modelled values are in general too high. The dissolved [Nd] model output for the same profile shows a good comparison with data. It is quite possible that this offset is due to additional input of highly radiogenic Nd from the New Zealand margin. Indeed this region is poorly constrained by the existing dissolved [Nd] and ϵ_{Nd} data. Alternatively the offset could be due to inadequacies in the tracer transport field or additional scavenging by POC. POC flux is high in this region and simulations we have carried out with increase scavenging by POC do indeed help improve the model-data comparison. We do not include these simulations here in order to be concise.

3.4. Further sensitivity tests

3.4.1. Sensitivity of Nd profiles to K_{ref}

The effect of doubling and halving K_{ref} on individual water-column profiles of dissolved [Nd] is shown in Figs. 6D and 7D by the black and grey lines respectively. Increasing K leads to increased dissolved [Nd] at depth. This sensitivity results from the use of fixed surface boundary conditions because increasing K_{ref} increases the flux of [Nd] away from the surface with the effect of increasing the dissolved [Nd] input to the surface ocean. This change in deep dissolved [Nd] is less strong in the North Atlantic (Fig. 6D), where transport of Nd along water-mass trajectories is most vigorous and affects deep dissolved [Nd]. In the North Pacific (Fig. 7D) the sensitivity of deep dissolved [Nd] to changes in K_{ref} is less pronounced because the scavenging of Nd by opal and dust does not lead to an increase in dissolved [Nd] with depth (see discussion in Section 2.2).

Increasing K_{ref} increases the rate at which Nd is moved down the water column. This emphasises the vertical transport of Nd via reversible scavenging compared to the lateral transport of Nd within water masses. The increased emphasis on vertical transport tends to make the transects of ϵ_{Nd} more uniform with respect to depth (i.e. reduces the range of ϵ_{Nd} in the profile) whereas decreasing K_{ref} increases the heterogeneity of ϵ_{Nd} in the vertical axis enhancing the signal of large-scale transport by ocean water masses (Figs. 6B and 7B). This effect is barely noticeable in the Atlantic (Fig. 6B) where the

transport within water masses is vigorous and lateral transport dominates even for doubling and halving K_{ref} , but it is a significant effect in the deep Pacific where deep ϵ_{Nd} values are sensitive to changes in K_{ref} (Fig. 7B).

3.4.2. Sensitivity to sea-floor dissolution

In order to consider the sensitivity of the model to the dissolution of particles at the sea floor we removed the sea-floor dissolution from the model and applied the same optimisation procedure as that described in Section 2.6.1. Under this alternative configuration optimum values are found of: $K_{\text{POC}}=0$; $K_{\text{CaCO}_3}=4.9 \times 10^5$; $K_{\text{dust}}=37.7 \times 10^5$ and; $K_{\text{opal}}=0.0 \times 10^5$. It is interesting to note that $K_{\text{POC}}=0$ in this configuration of the model and that K_{dust} remains relatively high. Both of these results are similar to the control optimisation and are therefore robust to the lack of sea-floor dissolution in this sensitivity test.

K_{CaCO_3} is higher for the case without dissolution at the sea floor ($K_{\text{CaCO}_3}=4.9 \times 10^5$ compared to $K_{\text{CaCO}_3}=2.6 \times 10^5$ in the control) and K_{opal} is almost zero ($K_{\text{opal}}=0.0 \times 10^5$ compared to $K_{\text{opal}}=4.1 \times 10^5$ in the control). This adjustment in K values implies that more of the vertical transfer of Nd in the ocean is achieved by scavenging by CaCO_3 compared to the control run and that scavenging by opal is ineffective. Significantly, without sea-floor dissolution the residence time for the optimised simulation is 360 yr, less than that of the control simulation. This is because, if one does not allow for dissolution at the sea floor, the sea floor becomes a more efficient sink for [Nd]. This effect is particularly significant for opal dissolution in the Southern Ocean. Opal dissolution in the Southern Ocean occurs mostly at the sea floor with relatively little dissolution occurring in the water column. In the absence of sea-floor dissolution the opal flux to the sediment removes Nd from the model very efficiently. This explains why the optimal K_{opal} is effectively zero for the case without sea-floor dissolution – the large reduction in the scavenging efficiency of opal is required so that the removal of Nd to the sediment by opal scavenging does not impact the residence time of Nd in the ocean.

Despite this important change to the residence time, the removal of sea-floor dissolution has no significant effect outside of the Southern Ocean for dissolved [Nd] and has no noticeable effect on ϵ_{Nd} anywhere. The blue line in the leftmost plot in Fig. 6D shows the effect of not allowing particle dissolution at the sea floor in the Southern Ocean. Reduced scavenging by opal means that less Nd is transferred to the deep Southern Ocean, reducing dissolved [Nd] there. This reduced scavenging and deep opal concentration in the Southern Ocean is required so that the residence time of Nd in the ocean is not greatly reduced due to removal via the opal flux to the sediment in the Southern Ocean.

In summary, dissolution at the sea floor significantly affects [Nd] in the deep Southern Ocean but has very little effect elsewhere in the ocean. This is because opal is subject to minimal dissolution in the water column in the Southern Ocean but dissolves significantly at the sea floor, unlike other particle types. Because most of the opal dissolution occurs at the sea floor it is important to represent sea-floor dissolution of opal. Without opal dissolution at the sea floor excessive amounts of Nd are removed in the Southern Ocean, reducing [Nd] there as well as the residence time of Nd in the ocean. Away from cold, high latitude waters such as those of the Southern Ocean, opal dissolution occurs dominantly in the water column and sea-floor dissolution is less important for the cycling of Nd in the water column.

4. Discussion

The results shown in Figs. 5, 6 and 7 suggest that reversible scavenging can help explain the difference between [Nd] and ϵ_{Nd} (i.e. the Nd paradox defined here), as evidenced in key ways:

1. modelled [Nd] concentrations are increased in the deep Pacific compared to the Atlantic (Fig. 5B), following similar trends in nutrient concentrations and observations and;

2. modelled [Nd] generally increases with depth while ε_{Nd} tracks a very different pattern driven by the circulation of deep-water masses and the ε_{Nd} signature of Nd inputs (Fig. 6A–D).

The decoupling of [Nd] and ε_{Nd} is particularly noticeable in the Atlantic where ε_{Nd} is strongly affected by water-mass transport but [Nd] is not (Fig. 6A–D). Why does a model that includes reversible scavenging capture these effects? This is explained as follows:

1. Reversible scavenging moves Nd to depth, where particle dissolution releases it such that [Nd] increases with depth. In a similar fashion nutrients are remineralised during particle dissolution. This explains the similarity between nutrient concentrations and [Nd] – both follow very similar transport pathways and tend to accumulate in the deep Pacific.
2. When sinking particles enter a new water mass with similar [Nd] but different ε_{Nd} the particles exchange isotopes without altering [Nd] concentrations – in this way reversible scavenging has important similarities with the process of boundary exchange described by Lacan and Jeandel (2005) and Arsouze et al. (2007).

Could significant groundwater discharge of Nd cause isotope variations without altering [Nd] (Johannesson and Burdige, 2007) and provide an alternative explanation for the Nd paradox? Although this effect should be considered in future models of Nd in the ocean, groundwater discharge of Nd it is difficult to conceive how such a mechanism would drive the observed systematic increase of Nd with respect to depth. Furthermore, it seems unlikely that significant groundwater discharge occurs at all depths and therefore we rule the possibility that groundwater discharge can explain the Nd paradox. We are not aware of alternative explanations to explain the observed increase of [Nd] with respect to depth besides reversible scavenging, which we show can explain many aspects of the Nd distribution in the ocean.

5. Closing comments

This work is intended to establish that reversible scavenging is a necessary component in explaining the marine Nd cycle and the so called Nd paradox, the decoupling of Nd concentrations and isotopes in the global ocean. Alternatives, such as non-reversible scavenging or significant submarine groundwater discharge (Johannesson and Burdige, 2007), cannot account for the observed increase in [Nd] with depth. From the model results shown here one may conclude that, on the broad scale, reversible scavenging is an active and important component in the cycling of Nd in the ocean. In particular, in the Atlantic reversible scavenging drives the increase in Nd with depth but also allows ε_{Nd} to act as an effective water-mass tracer. Nd accumulates in the deep Pacific in a similar way to nutrients. Therefore reversible scavenging can help explain the Nd paradox. Because the model is tuned to optimise the fit to $\sigma_{[\text{Nd}]}$, the fact that the model represents ε_{Nd} reasonably well is an independent validation of the importance of reversible scavenging for modelling Nd in the ocean.

The effect of particle type on scavenging of [Nd] is significant because dissolution profiles differ significantly for different particle types. Any change in scavenging efficiency between particle types therefore has an important impact on profiles of [Nd] because these are closely coupled to dissolution. We emphasise the need for observational constraints on the scavenging coefficients of different particle types, either derived from laboratory experiments or field observations as well as improved constraints on particle dissolution profiles.

The effectiveness of ε_{Nd} as a water-mass tracer reflects the balance between the rate of ocean transport compared to the rate of transfer of ε_{Nd} down the water column via reversible scavenging. In the Atlantic, distinct and relatively fast-moving water masses shift this balance in favour of ε_{Nd} acting as a water-mass tracer. In the Pacific water masses are more sluggish and ε_{Nd} profiles more uniform with respect to depth,

reflecting the increased influence of reversible scavenging in this basin (compare Figs. 6B and 7B, note that the horizontal scales are different in each plot). The impact of the rate of ocean transport on the effectiveness of Nd as a water-mass tracer is significant. During periods of reduced deep-water circulation in the North Atlantic (see, e.g. McManus et al., 2004) Nd is more likely to be removed to the sea floor there than to undergo lateral transport. Such an effect may be significant in interpreting downcore records of ε_{Nd} such as that of Piotrowski et al. (2005).

Although the inclusion of reversible scavenging explains many aspects of the paradox, remaining questions exist and the approach we present here cannot be considered fully quantitative because of the use of an over-simplified fixed surface boundary condition. Tachikawa et al. (2003) discuss considerably more sophisticated source terms than that included in the current study. Further careful studies of the input of Nd into the ocean will need to be carried out in the future.

Lacan and Jeandel (2005) and Arsouze et al. (2007) emphasise the importance of the exchange of Nd isotopes with ocean margins via the process of boundary exchange. For the purpose of the present process study into reversible scavenging we have not included boundary exchange but an obvious next step will be to include boundary exchange in our model. Throughout the text we point out parallels between boundary exchange and reversible scavenging that suggest a possible explanation for the depth-dependency of boundary exchange and it will be interesting to test this hypothesis in a more complete model that includes boundary exchange. We tentatively suggest here that the inclusion of boundary exchange in the deep Pacific may help to reconcile the model results with the high ε_{Nd} values which are observed there.

Acknowledgements

Significant guidance and insight was generously provided by Martin Frank, Alex Piotrowski, Thomas Stocker and Andy Ridgwell. Martin Frank also provided data compilations. SK was funded by NSF grant OCE-0623366. This work was partially funded by NSF grant OCE 05-26884 to SLG and SRH. TvdF acknowledges support from OCE 0623107. Support from the Lamont Doherty Earth Observatory of Columbia University and the University of Bristol is gratefully acknowledged.

References

- Albarède, F., Goldstein, S.L., 1992. A world map of Nd isotopes in seafloor ferromanganese deposits. *Geology* 20, 761–763.
- Amakawa, H., Alibo, D.S., Nozaki, Y., 2000. Nd isotopic composition and REE pattern in the surface waters of the eastern Indian Ocean and its adjacent seas. *Geochim. Cosmochim. Acta* 64, 1715–1727.
- Amakawa, H., Alibo, D.S., Nozaki, Y., 2004. Nd concentration and isotopic composition distributions in the surface waters of the Northwest Pacific Ocean and its adjacent seas. *Geochem. J.* 38, 493–504.
- Archer, D., 1996. A data-driven model of the global calcite lysocline. *Glob. Biogeochem. Cycles* 10 (3), 511–526.
- Arsouze, T., Dutay, J.C., Lacan, F., Jeandel, C., 2007. Modeling the neodymium isotopic composition with a global ocean general circulation model. *Chem. Geol.* 239 (1–2), 156–164.
- Arsouze, T., Dutay, J.C., Kageyama, M., Lacan, F., Alkama, R., Marti, O., Jeandel, C., 2008. Influence of the Atlantic thermohaline circulation on neodymium isotopic composition at the Last Glacial Maximum – a modelling sensitivity study. *Clim. Past Discuss.* 4, 309–333.
- Bacon, M.P., Anderson, R.F., 1982. Distribution of thorium isotopes between dissolved and particulate forms in the deep sea. *J. Geophys. Res.* 87, 2045–2056.
- Bayon, G., German, C.R., Burton, K.W., Nesbitt, R.W., Rogers, N., 2004. Sedimentary Fe–Mn oxyhydroxides as paleoceanographic archives and the role of aeolian flux in regulating oceanic dissolved REE. *Earth Planet. Sci. Lett.* 224 (3–4), 477–492.
- Behrenfeld, M.G., Falkowski, P.G., 1997. Photosynthetic rates derived from satellite-based chlorophyll concentration. *Limnol. Oceanogr.* 42, 1–20.
- Bertram, C.J., Elderfield, H., 1993. The geochemical balance of the rare earth elements and neodymium isotopes in the oceans. *Geochim. Cosmochim. Acta* 57, 1957–1986.
- Broecker, W.S., Peng, T.H., 1982. *Tracers in the Sea*. Eldigio Press, New York.
- Chase, Z., Anderson, R.F., Fleisher, M.Q., Kubik, P.W., 2002. The influence of particle composition and particle flux on scavenging of Th, Pa and Be in the ocean. *Earth Planet. Sci. Lett.* 204, 215–219.
- de Baar, H.J.W., Bacon, M.P., Brewer, P.G., Bruland, K.W., 1985. Rare earth elements in the Pacific and Atlantic Oceans. *Geochim. Cosmochim. Acta* 49, 1943–1959.

- Dutay, J.C., et al., 2002. Evaluation of ocean model ventilation with CFC-11: comparison of 13 global ocean models. *Ocean Modelling* 4 (2), 89–120.
- Elderfield, H., 1988. The oceanic chemistry of the rare-earth elements. *Phil. Trans. Roy. Soc. London Ser. A: Math. Phys. Eng. Sci.* 325 (1583), 105–126.
- Elderfield, H., Greaves, M.J., 1982. The rare-earth elements in sea-water. *Nature* 296 (5854), 214–219.
- Elderfield, H., Sholkovitz, E.R., 1987. Rare earth elements in the pore waters of reducing nearshore sediments. *Earth Planet. Sci. Lett.* 82, 280–288.
- Frank, M., 2002. Radiogenic isotopes: tracers of past ocean circulation and erosional input. *Rev. Geophys.* 40. doi:10.1029/2000RG000094.
- Gent, P.R., McWilliams, J.C., 1990. Isopycnal mixing in ocean circulation models. *J. Phys. Oceanogr.* 20, 150–155.
- German, C.R., Klinkhammer, G.P., Edmond, J.M., Mitra, A., Elderfield, H., 1990. Hydrothermal scavenging of rare-earth elements in the ocean. *Nature* 345, 516–518.
- German, C.R., Masuzawa, T., Greaves, M.J., Elderfield, H., Edmond, J.M., 1995. Dissolved rare-earth elements in the southern-ocean – cerium oxidation and the influence of hydrography. *Geochim. Cosmochim. Acta* 59 (8), 1551–1558.
- Ginoux, P., Chin, M., Tegen, I., Prospero, J., Holben, B., Dubovik, O., Lin, S.J., 2001. Sources and global distributions of dust aerosols simulated with the GOCART model. *J. Geophys. Res.* 106 (20), 255–273.
- Greaves, M.J., Elderfield, H., Sholkovitz, E.R., 1999. Aeolian sources of rare earth elements to the Western Pacific Ocean. *Mar. Chem.* 68 (1–2), 31–38.
- Goldstein, S.L., O’Nions, R.K., 1981. Nd and Sr isotopic relationships in pelagic clays and ferromanganese deposits. *Nature* 292, 324–327.
- Goldstein, S.L., Hemming, S.R., 2003. Long-lived isotopic tracers in oceanography, paleoceanography, and ice-sheet dynamics. In: Elderfield, H. (Ed.), *Treatise on Geochemistry*. Elsevier, Oxford.
- Halliday, A.N., Davidson, J.P., Holden, P., Owen, R.M., Olivarez, A.M., 1992. Metalliferous sediments and the scavenging residence time of Nd near hydrothermal vents. *Geophys. Res. Lett.* 19, 761–764.
- Henderson, G.M., Heinze, C., Anderson, R.F., Winguth, A.M.E., 1999. Global distribution of the ^{230}Th flux to ocean sediments constrained by GCM modelling. *Deep-Sea Research* 1 46, 1861–1894.
- Jacobsen, S.B., Wasserburg, G.J., 1980. Sm–Nd isotopic evolution of chondrites. *Earth Planet. Sci. Lett.* 50, 139–155.
- Jeandel, C., 1993. Concentration and isotopic composition of Nd in the South Atlantic Ocean. *Earth Planet. Sci. Lett.* 117, 581–591.
- Jeandel, C., Thouron, D., Fioux, M., 1998. Concentrations and isotopic compositions of neodymium in the Eastern Indian Ocean and Indonesian straits. *Geochim. Cosmochim. Acta* 62, 2597–2607.
- Jeandel, C., Bishop, J.K., Zindler, A., 1995. Exchange of neodymium and its isotopes between seawater and small and large particles in the Sargasso Sea. *Geochim. Cosmochim. Acta* 59, 535–547.
- Jiang, S., Stone, P.H., Malanotte-Rizzoli, P., 1999. An assessment of the Geophysical Fluid Dynamics Laboratory ocean model with coarse resolution: annual-mean climatology. *J. Geophys. Res.* 104 (C11), 25623–25645.
- Johannesson, K.H., Burdige, D.J., 2007. Balancing the global oceanic neodymium budget: evaluating the role of groundwater. *Earth Planet. Sci. Lett.* 253 (1–2), 129–142.
- Jones, K.M., Khatiwala, S.P., Goldstein, S.L., Hemming, S.R., van de Fliert, T., 2008. Modeling the distribution of Nd isotopes in the oceans using an ocean general circulation model. *Earth Planet. Sci. Lett.* 272 (3–4), 610–619.
- Jones, K., Khatiwala, S., van de Fliert, T., Hemming, S.R., Goldstein, S.L., Modeling the isotopic composition of Nd in the ocean: impact of surface sources and boundary exchange, in press.
- Khatiwala, S., 2007. A computational framework for simulation of biogeochemical tracers in the ocean. *Glob. Biogeochem. Cycles* 21, GB3001. doi:10.1029/2007GB002923.
- Khatiwala, S., Visbeck, M., Cane, M.A., 2005. Accelerated simulation of passive tracers in ocean circulation models. *Ocean Modelling* 9, 51–69.
- Lacan, F., Jeandel, C., 2001. Tracing Papua New Guinea imprint on the central Equatorial Pacific Ocean using neodymium isotopic compositions and Rare Earth Element patterns. *Earth Planet. Sci. Lett.* 186, 497–512.
- Lacan, F., Jeandel, C., 2005. Neodymium isotopes as a new tool for quantifying exchange fluxes at the continent–ocean interface. *Earth Planet. Sci. Lett.* 232, 245–257.
- Laws, E.A., Falkowski, P.G., Smith Jr., W.O., Ducklow, H., McCarthy, J.J., 2000. Temperature effects on export production in the open ocean. *Glob. Biogeochem. Cycles* 14, 1231–1246.
- Levitus, S., 1998. *World Ocean Database 1998*, NOAA Atlas NESDIS, 18. US Government Printing Office, Washington, DC.
- Maier-Reimer, E., 1993. Geochemical cycles in an ocean general circulation model: preindustrial tracer distributions. *Glob. Biogeochem. Cycles* 7, 645–677.
- Marchal, O., François, R., Stocker, T.F., Joos, F., 2000. Ocean thermohaline circulation and sedimentary $^{231}\text{Pa}/^{230}\text{Th}$ ratio. *Paleoceanography* 15, 625–641.
- Marshall, J., Adcroft, A., Hill, C., Perelman, L., Heisey, C., 1997. A finite-volume, incompressible Navier Stokes model for studies of the ocean on parallel computers. *J. Geophys. Res.* 102, 5753–5766.
- Matsumoto, K., et al., 2004. Evaluation of ocean carbon cycle models with data-based metrics. *Geophys. Res. Lett.* 31 (7), L07303.
- McManus, J.F., Francois, R., Gherardi, J.M., Keigwin, L.D., Brown-Leger, S., 2004. Collapse and rapid resumption of Atlantic meridional circulation linked to deglacial climate changes. *Nature* 428, 834–837.
- Piegras, D.J., Wasserburg, G.J., 1980. Neodymium isotopic variations in seawater. *Earth Planet. Sci. Lett.* 50, 128–138.
- Piegras, D.J., Wasserburg, G.J., 1982. Isotopic composition of neodymium in waters from the Drake Passage. *Science* 217, 207–214.
- Piegras, D.J., Wasserburg, G.J., 1983. Influence of the Mediterranean outflow on the isotopic composition of neodymium in waters of the North-Atlantic. *J. Geophys. Res.* 88, 5997–6006.
- Piegras, D.J., Wasserburg, G.J., 1985. Strontium and neodymium isotopes in hot springs on the East Pacific Rise and Guaymas Basin. *Earth Planet. Sci. Lett.* 72, 341–356.
- Piegras, D.J., Wasserburg, G.J., 1987. Rare earth element transport in the western North Atlantic inferred from Nd isotopic observations. *Geochim. Cosmochim. Acta* 51, 1257–1271.
- Piegras, D.J., Jacobsen, S.B., 1988. The isotopic composition of neodymium in the North Pacific. *Geochim. Cosmochim. Acta* 52, 1373–1381.
- Piegras, D.J., Jacobsen, S.B., 1992. The behavior of rare-earth elements in seawater – precise determination of variations in the north pacific water column. *Geochim. Cosmochim. Acta* 56 (5), 1851–1862.
- Piegras, D.J., Wasserburg, G.J., Dasch, E.J., 1979. The isotopic composition of Nd in different ocean masses. *Earth Planet. Sci. Lett.* 45, 223–236.
- Piotrowski, A.M., Goldstein, S.L., Hemming, S.R., Fairbanks, R.G., 2004. Intensification and variability of ocean thermohaline circulation through the last deglaciation. *Earth Planet. Sci. Lett.* 225, 205–220.
- Piotrowski, A.M., Goldstein, S.L., Hemming, S.R., Fairbanks, R.G., 2005. Temporal relationships of carbon cycling and ocean circulation at glacial boundaries. *Science* 307, 1933–1938.
- Ridgwell, A., Hargreaves, J., 2007. Regulation of atmospheric CO_2 by deep-sea sediments in an Earth System Model. *Glob. Biogeochem. Cycles* 21. doi:10.1029/2006GB002764.
- Ridgwell, A.J., Watson, A.J., Archer, D.A., 2002. Modelling the response of the oceanic Si inventory to perturbation and consequences for atmospheric CO_2 . *Glob. Biogeochem. Cycles* 16. doi:10.1029/2002GB001877.
- Rutberg, R.L., Hemming, S.R., Goldstein, S.L., 2000. Reduced North Atlantic Deep Water flux to the glacial Southern Ocean inferred from neodymium isotope ratios. *Nature* 405 (6789), 935–938.
- Shimizu, H., Tachikawa, K., Masuda, A., Nozaki, Y., 1994. Cerium and neodymium isotope ratios and REE patterns in seawater from the north Pacific-Ocean. *Geochim. Cosmochim. Acta* (1), 323–333.
- Sholkovitz, E.R., Elderfield, H., Szymczak, R., Casey, K., 1999. Island weathering: river sources of rare earth elements to the Western Pacific Ocean. *Mar. Chem.* 68, 39–57.
- Sholkovitz, E.R., Szymczak, R., 2000. The estuarine chemistry of rare earth elements: comparison of the Amazon, Fly, Sepik and the Gulf of Papua systems. *Earth Planet. Sci. Lett.* 179, 299–309.
- Siddall, M., Henderson, G.M., Edwards, N.R., Müller, S.A., Stocker, T.F., Joos, F., Frank, M., 2005. $^{231}\text{Pa}/^{230}\text{Th}$ fractionation by ocean transport, biogenic particle flux and particle type. *Earth Planet. Sci. Lett.* 237, 137–155.
- Siddall, M., Stocker, T.F., Henderson, G.M., Joos, F., Frank, M., Edwards, N.R., Ritz, S., Müller, S.A., 2007. Modelling the relationship between $^{231}\text{Pa}/^{230}\text{Th}$ distribution in the North Atlantic sediment and Atlantic Meridional Overturning Circulation. *Paleoceanography* 22, No.2, PA2214. doi:10.1029/2006PA001358.
- Siddall, M., Anderson, R.F., Winckler, G., Henderson, G.M., Bradtmiller, L.L., McGee, D., Franzese, A., Stocker, T.F., Müller, S.A., 2008. Modelling the particle-flux effect on distribution of ^{230}Th in the equatorial Pacific. *Paleoceanography* 23, PA2208. doi:10.1029/2007PA001556.
- Spivack, A.J., Wasserburg, G.J., 1988. Neodymium isotopic composition of the Mediterranean outflow and the eastern North Atlantic. *Geochim. Cosmochim. Acta* 52, 2767–2773.
- Tachikawa, K., Jeandel, C., Roy-Barman, M.A., 1999. new approach to the Nd residence time in the ocean: the role of atmospheric inputs. *Earth Planet. Sci. Lett.* 170 (4), 433–444.
- Tachikawa, K., Athias, V., Jeandel, C., 2003. Neodymium budget in the modern ocean and paleo-oceanographic implications. *J. Geophys. Res.* 108. doi:10.1029/1999JC000285.
- Taylor, S.R., McLennan, S.M., 1985. *The Continental Crust: Its Composition and Evolution*. Blackwell, Oxford.
- Trenberth, K.E., Large, W.G., Olson, J.G., 1989. A global ocean wind stress climatology based on ECMWF analyses. TN-338+STR, National Center for Atmospheric Research. 93 pp.
- Treguer, P., Nelson, D.M., VanBennekom, A.J., Demaster, D.J., Leynaert, A., Queguiner, B., 1995. The silica balance in the world ocean – a reestimate. *Science* 268 (5209), 375–379.
- van de Fliert, T., Frank, M., Lee, D.C., Halliday, A.N., Reynolds, B.C., Hein, J.R., 2004. New constraints on the sources and behavior of neodymium and hafnium in seawater from Pacific Ocean ferromanganese crusts. *Geochim. Cosmochim. Acta* 68, 3827–3843.
- van de Fliert, T., Robinson, L.F., Adkins, J.F., Hemming, S.R., Goldstein, S.L., 2006. Temporal stability of the neodymium isotope signature of the Holocene to glacial North Atlantic. *Paleoceanography* 21, PA4102. doi:10.1029/2006PA001294.
- Vance, D., Scrivner, A.E., Beney, P., Staubwasser, M., Henderson, G.M., Slowey, N.C., 2004. The use of foraminifera as a record of the past neodymium isotope composition of seawater. *Paleoceanography* 19. doi:10.1029/2003PA000957.
- von Blanckenburg, F., 1999. Tracing past ocean circulation. *Science* 286, 1862–1863.